# Nanoscale detection and real-time monitoring of free radicals in a single living cell under the stimulation of targeting moieties using a nanodiamond quantum sensor

Kaiqi Wu [a]†, Qi Lu[a] †, Maabur Sow [b], Priyadharshini Balasubramanian [b], Fedor Jelezko [b], Tanja Weil [a]*, Yingke Wu [a]*

[a] Max Planck Institute for Polymer Research, Ackermannweg 10, 55128 Mainz, Germany

*E-mail: weil@mpip-mainz.mpg.de, wuyingke@mpip-mainz.mpg.de.

[b] Institute for Quantum Optics and Center for Integrated Quantum Science and Technology (IQST), Ulm University, Albert-Einstein-Allee 11, 89081 Ulm, Germany

Keywords: Nanodiamond, cell targeting peptides, in-cell free radicals detection, nitrogen-vacancy center, quantum sensor, $T_1$ relaxometry

†Kaiqi Wu and Qi Lu contributed equally.

## Abstract

Intracellular radicals play important roles in cell signaling and regulation of growth factors, cytokines, transcription, apoptosis, and immunomodulation, among others. To gain a more comprehensive understanding of their biological functions in a spatio-temporal perspective, there is a great need for nanoscale sensitive tools that allow real-timeiin detection of these reactive species. Currently, intracellular radical probes are based on chemical reactions that could significantly alter radical levels during detection. Due to the excellent biocompatibility and favorable photophysical properties of nitrogen-vacancy ($NV^-$) centers in fluorescent nanodiamonds (fNDs), the fNDs can serve as a powerful and chemically inert nanotool for intracellular radical detection. In this study, a positively charged nanogel (NG) coating was prepared to prevent the precipitation of fNDs and promote cellular internalization. After internalization of nanodiamond-nanogels (fND-NGs), different stimulators, namely somatostatin (SST), triphenylphosphonium (TPP), and trans-activator of transcription (TAT) peptide, which are widely used cell- or organelle- targeting ligands in medicine, drug delivery, and diagnostics, were applied to stimulate the cells. In parallel, the intracellular radical changes under stimulation of SST, TPP, and TAT ligands were monitored by fND-NGs in a home-built ODMR microscope. Our method allows for detecting intracellular radicals *in-situ* and monitoring their real-time changes during incubation with the targeting ligands in a single living cell. We believe that our method will provide insights into the generation of radical stress in cells, which could improve our fundamental understanding of the pharmacology and signaling pathways of widely used cell- and organelle-targeting ligands associated with free radicals.

## Introduction

Free radicals in biology were historically regarded as villains contributing to a spectrum of pathological disorders, including cancers, diabetes, cardiovascular maladies, and various others.[1,2] For instance, free radical-mediated reactions could induce chromosomal aberrations, facilitate the activation of oncogenic elements, and consequently culminate in tumorigenesis.[3] On the contrary, it is also found that free radicals can play several beneficial roles in many biological processes when maintained at low or moderate concentrations.[4,5] For example, reactive oxygen species (ROS) and reactive nitrogen species (RNS) generated in phagocytes assist the host immune defense system in combating pathogens.[6,7] Therefore, *in-situ* detection of free radicals is essential to elucidate their diverse roles in cells.

However, *in-situ* detection of intracellular radicals is still in its infancy as we lack the appropriate techniques to study their formation, lifetime, and interaction partners. Current methods for detecting intracellular radicals are mainly based on fluorescence-based dyes, such as amino/hydroxyphenyl fluorescein.[8] However, these dyes chemically react with the radicals in the detection, which at the same time alters their amount.[9,10] Fluorescent nanodiamonds (fNDs) containing nitrogen-vacancy ($NV^-$) centers could provide sensitive detection of intracellular radicals without involving chemical reactions due to their unique photophysical properties.[11,12] The longitudinal relaxation time ($T_1$) of the $NV^-$ centers in fNDs can be shortened by the surrounding magnetic noise which is generated by the electron spins of radicals. Based on this photophysical property, fNDs-based $T_1$ relaxometry was developed to locally detect and quantify radicals.[13] Additionally, fNDs offer distinct advantages in terms of biocompatibility[14], sensitivity[15], and resolution[16] compared to fluorescent probes. Internalized fNDs also do not react with radicals and do not bleach, which enables real-time long-duration measurements.[17] Recently, $T_1$ relaxometry has successfully been used to investigate metabolic activity and radical formation in living cells.[18] For example, cellular metabolic activities in single mitochondria were monitored using $T_1$ relaxometry. An increase of intracellular radicals was observed upon carbonyl cyanide *m*-chlorophenyl hydrazone treatment, whereas a decrease of radical levels occurred upon superoxide dismutase treatment.[19] Moreover, $T_1$ relaxometry was utilized to detect the host cellular radical response upon Semliki Forest Virus[20] and *S.aureus*[21] infections. Very recently, a fND-based radical generator and detector was reported.

Such system allowed quantifying the local number and kinetics of free radicals generated in an eumelanin shell inside cells by combining experiments and theoretical simulations.[22] This study provides a perspective toward quantifying radicals in the living environment.

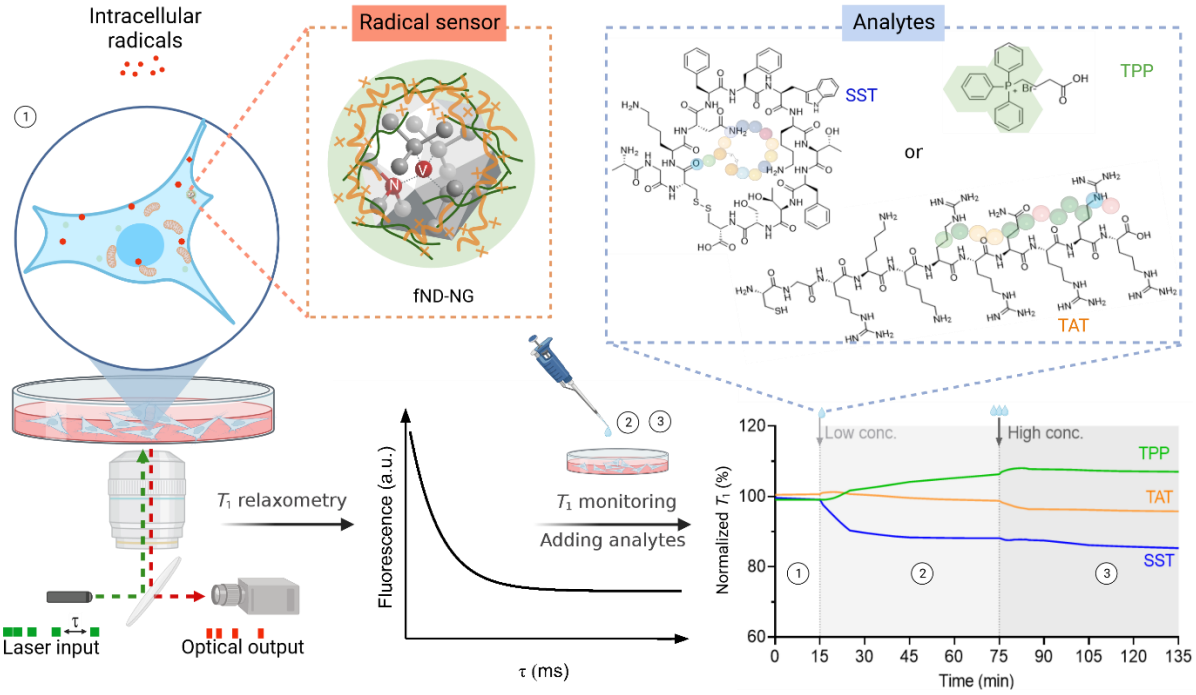


**Scheme 1.** Detecting cellular radical responses of A549 cells upon incubation with ligands SST, TPP, and TAT. fND-NGs were first incubated with the cell to perform $T_1$ relaxometry measurements and then low and high ligand concentrations were added to the ongoing $T_1$ relaxometry measurements at 15 min and 75 min time points. τ indicates the waiting time of the laser pulses. Stage ① indicates the cellular intrinsic free radicals, and stage ②, ③ represent cellular radical responses upon treatment with low and high ligand concentrations, respectively.

In this work, a positively charged nanogel (NG) coating was prepared to prevent the precipitation of fNDs according to our previous work[23,24] and promote cellular internalization. Subsequently, intracellular localization of fND nanogel (fND-NGs) were characterized utilizing confocal microscopy and quantified by employing Manders' Colocalization Coefficients (MCC). Later, internalized fND-NGs were applied to optically probe the free radical response of human lung carcinoma cells (A549) in response to three commonly used targeting ligands, i.e. growth factor peptide somatostatin (SST)[25], mitochondrial targeting ligand triphenylphosphonium (TPP)[26] or

trans-activator of transcription (TAT) peptide[27], assess their role in the formation and annihilation of intracellular radicals. By using our method, we could *in-situ* real-time monitor the intracellular radical generation/reduction upon treatment of widely used targeting groups. We believe our method will further our understanding of the fundamental role of various biomolecules and drugs in the formation and annihilation of free radicals in biology.

## Results and discussion

*Preparation and characterization of fND-NGs*

Bare fNDs have poor colloidal stability and aggregate under physiological conditions.[28] To address this challenge, we prepared fND-NGs according to previously published protocols.[23,24] In brief, hyperbranched polyethyleneimine (PEI) was used to pre-coat fNDs in the presence of polyvinylpyrrolidone (PVP) as a stabilizer. Subsequently, a four-arm polyethylene glycol-*N*-hydroxysuccinimide ester (4-arm PEG-SCM ester) was added, to crosslink the pre-coated PEI on the surface of the fNDs in phosphate-buffered saline (PBS) to form a stable, positively charged nanogel shell (as illustrated in **Figure 1A**). The nanogel shell was characterized by attenuated total reflectance Fourier-transform infrared spectroscopy (ATR-FTIR). Specifically, the presence of alky C–H ($\nu$: 2914 $cm^{-1}$, 2848 $cm^{-1}$, $\delta$: 1445-1311 $cm^{-1}$), amine (N–H ($\delta$): 1622-1500 $cm^{-1}$; C–N ($\delta$): 1240 $cm^{-1}$), and amide group (C=O ($\nu$): 1656 $cm^{-1}$) band originating from PEG and PEI (**Figure 1B**) indicated their successful conjugation to the fNDs surface. The hydrodynamic diameter of the fND-NGs was determined through dynamic light scattering (DLS) and transmission electron microscopy (TEM). After surface coating, the hydrodynamic diameter showed an increase of approximately 14 nm (from 42 nm to 56 nm, **Table S1**). Importantly, no aggregate formation of the fND-NGs was detected in either DLS or TEM (**Figure 1C-E**).

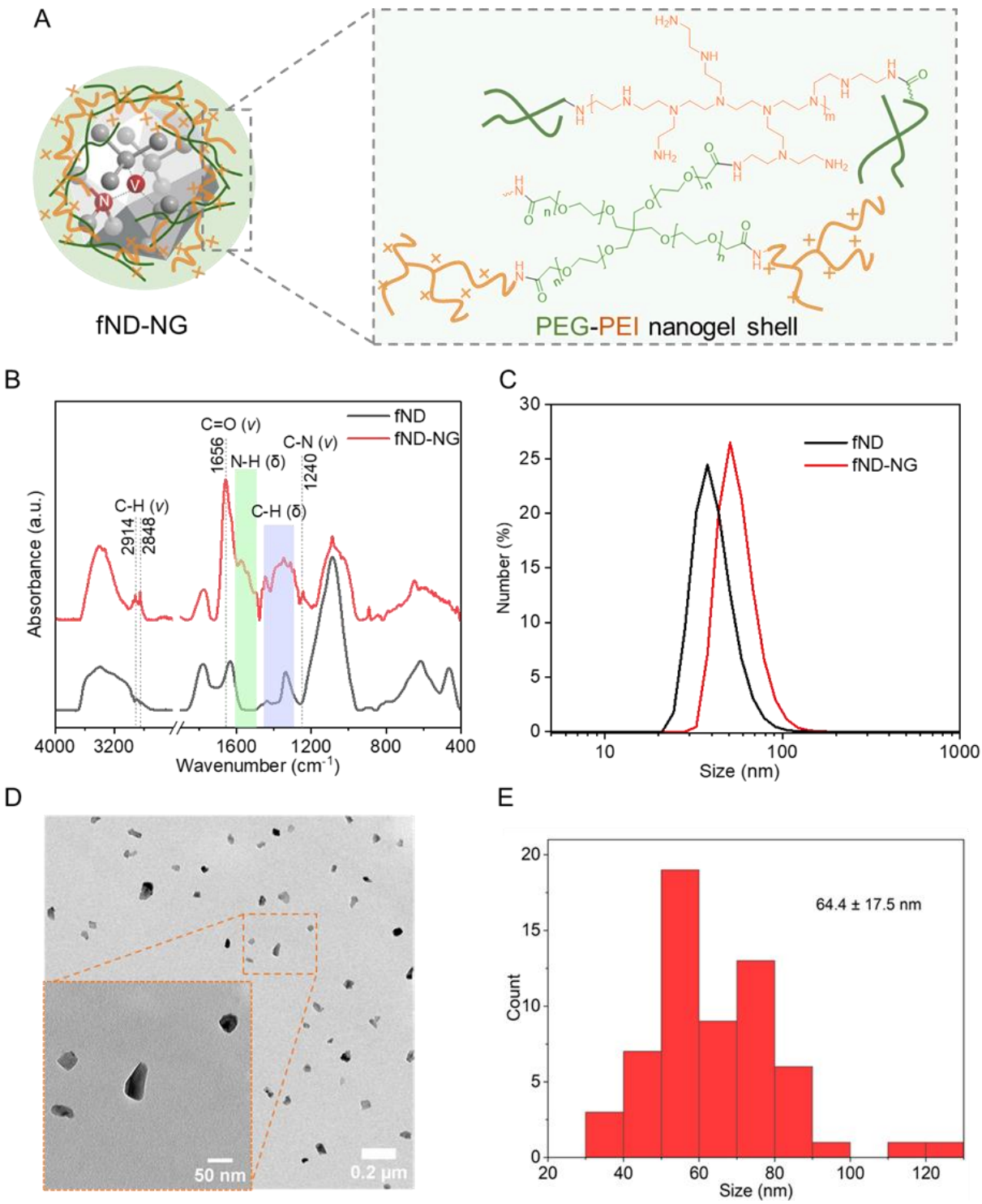


**Figure 1.** Characterization of fND-NGs. (A) Schematic structure of the fND-NGs shell. (B) ATR-FTIR of fNDs and fND-NGs. *ν*: stretching vibration; *δ*: bending vibration. (C) Number–size histogram of fND-NGs measured by DLS. (D) Representative TEM images of fND-NGs. (E) Diameter histogram analysis of fND-NGs measured by TEM (n = 60).

*Bioactive ligands SST, TPP, and TAT*

SST is a naturally occurring peptide hormone that plays a regulatory role in various physiological processes, including neurotransmission, hormone secretion, and cell proliferation.[29] SST receptors (SSTRs) are present on the surface of many cell types, including immune cells, neuronal cells, and certain cancer cells.[25,30] Therefore, the A549 epithelial cell line with SSTR1 and SSTR3 subtype expression was used in this study.[31] The specific binding property between SST and SSTRs is utilized for improved cancer detection and selectively therapeutic purposes.[32,33] Additionally, after binding to SSTRs, SST regulates nitric oxide (NO) generation through the activation of nitric oxide synthases (NOS) followed by triggering intracellular signaling pathways.[34] NO is a principal modulator of cellular processes in diverse physiological and pathological contexts.[35]

TPP ligand selectively accumulates within the mitochondria of cells. This specific targeting property is attributed to the mitochondrial membrane's negative potential, which facilitates the uptake and accumulation of lipophilic cations.[26] The TPP ligand has been reported to disrupt mitochondrial function by inhibiting oxidative phosphorylation, a known process capable of generating free radicals, such as superoxide ion ($\bullet O_2^-$) and hydroxyl free radicals (•OH).[36] Once delivered to the mitochondria, TPP molecules can engage in various bioenergetic and therapeutic applications.[37]

The TAT peptide is a positively charged amino acid sequence derived from the human immunodeficiency virus 1 (HIV-1) protein.[38,39] This unique peptide sequence efficiently crosses cellular membranes, making it a valuable tool in various biomedical applications.[27] TAT demonstrates a high degree of biocompatibility with no compromise in cell viability of A549 even at high concentrations of 1 mM.[40] TAT uses a non-endocytic, direct translocation mechanism that allows it to penetrate the lipid bilayer of the cell membrane without causing significant membrane damage[27,41] and is not involved in processes directly regulating intracellular radicals. Therefore, TAT has been selected as a potential negative control.

The cellular toxicity of SST, TPP, and TAT on A549 cell lines was evaluated using the cell-titer assay. As indicated in **Figure S1**, these targeting ligands did not

show any significant cellular toxicity for concentrations up to 100 µM (for SST and TAT) or 1mM (for TPP), which is consistent with the reported studies.[30,37,40]

*Subcellular location of fND-NGs*

In order to detect the formation of intracellular radicals upon incubation with SST, TPP, and TAT, the subcellular location of fND-NGs was first characterized by a confocal microscope. Firstly, the fND-NGs, at concentrations of 5 and 10 µg/mL, respectively, were incubated with A549 cells for 24 hours. Subsequently, lysosomes were stained using 50 nM lysotracker and incubated for an additional two hours at 37°C under a 5% $CO_2$ atmosphere. Following a thorough washing and medium replacement procedure, live cell imaging was conducted utilizing fluorescence confocal microscopy (**Figure 2**). The acquired images were de-convolved through a calculated point spread function using Fiji.[42] The colocalization ratio of fND-NGs and lysosomes was calculated by a pixel-level based MCC.[43,44] The proportion of colocalized fND-NGs, which was described by M1, was calculated by JACoP[45] using Fiji as:

$$M1 = \frac{\sum_i R_{i,colcoal}}{\sum_i R_i}$$

For two probes, denoted as R (Red, fND-NGs) and G (Green, lysotracker), $R_{i,\ colocal}$ = Ri if $G_i > 0$ and $R_{i,\ colocal} = 0$ if $G_i = 0$. The thresholds of both lysosomes and fND-NGs channels were determined from the maximum intensity of the control group images. The M1 for the cells incubated with 5 µg/mL and 10 µg/mL fND-NGs was around 0.15 and 0.04, which indicated that most of the particles likely escaped from lysosomal compartments and went to the cytoplasm. This feature could probably be attributed to the proton sponge effect of PEI,[46] which is positively charged in acidic endosomal or lysosomal compartments and promotes escaping into the cytoplasm. Therefore, we supposed the $T_1$ relaxometry measurements were performed in the cytoplasm.

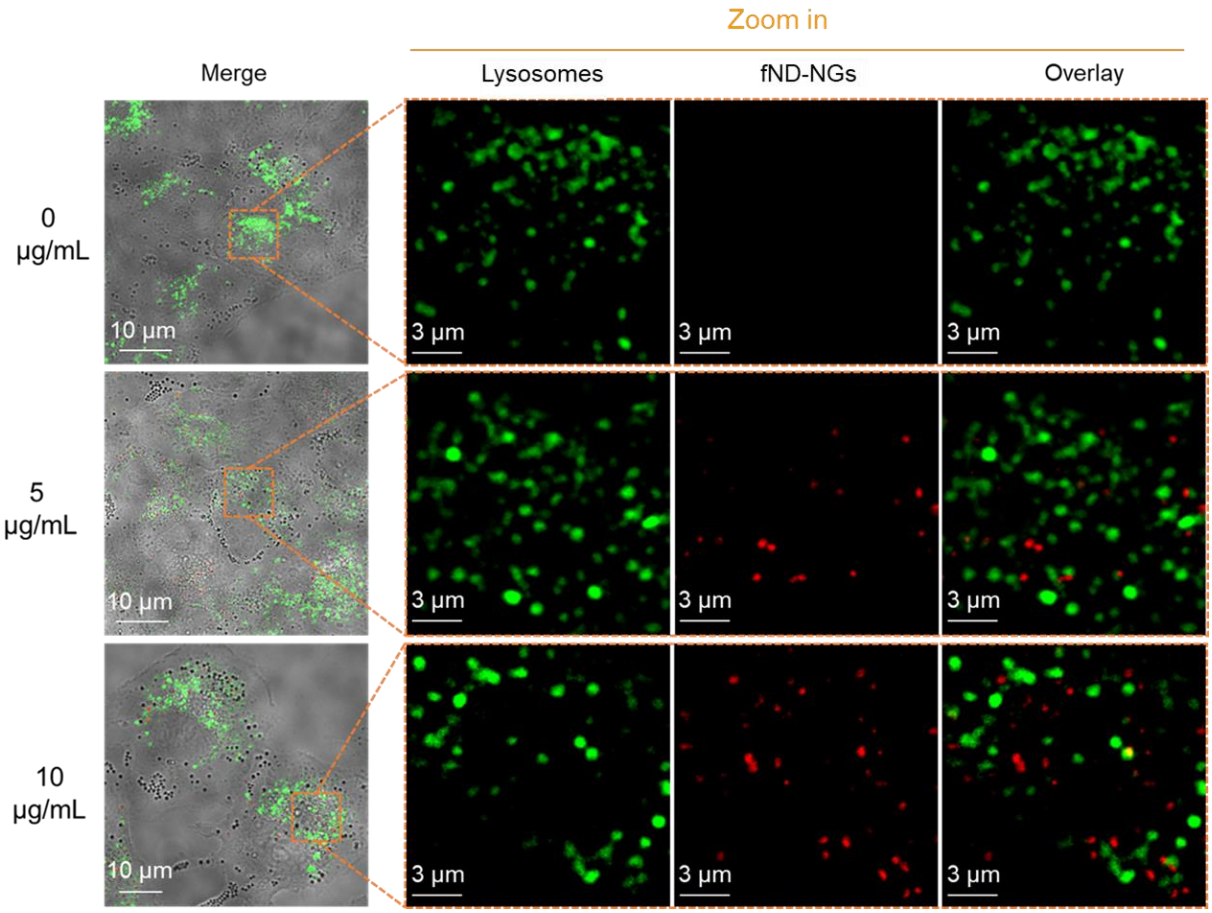


**Figure 2**. CLSM images of fND-NGs (red color) in A549 cells. fND-NGs were incubated with A549 cell lines for 24 h, then lysosomes were stained by Lyso-tracker (green color).

*Intracellular $T_1$ relaxometry*

To detect the presence of intracellular radicals, we utilized a home-built confocal fluorescence microscope combined with optically detected magnetic resonance (ODMR) spectroscopy driven by the software Qudi[47] for measurement. The $NV^-$ centers in fNDs were excited using a 532 nm laser, which was focused onto the sample using an oil-immersion objective (Nikon PLAN 100x oil, N.A. = 1.35). The resulting fluorescence originating from the $NV^-$ centers was collected by the same objective and filtered with a 740/75 nm band-pass filter and detected using an avalanche photodiode (APD).

The pulse sequence for the $T_1$ relaxometry measurement consists of a series of 10 μs long laser pulses. The laser pulse polarizes the $NV^-$ centers into the ms = 0 spin state. After a variable waiting time (τ), the subsequent laser pulse reads out the

spin state of the $NV^-$ centers. $T_1$ was measured using this all-optical relaxometry technique. The fluorescence photons detected in the first 300–500 ns of the laser pulse contain the spin state information and hence constitute the signal. The $T_1$ measurement data shown are normalized, i.e., the signal (fluorescence obtained during the first 300 ns) is divided by the reference steady-state fluorescence (fluorescence obtained when the $NV^-$ center is re-initialized into the ms = 0 spin state). Then, it is fitted with a monoexponential decay function. When fNDs were exposed to a fluctuating magnetic field produced by the surrounding radicals, the $T_1$ of $NV^-$ centers is shortened.[13] Therefore, determination of the concentration of radicals surrounding the fNDs surface can be achieved with high sensitivity and high spatial resolution. Recently, it was reported that $T_1$ relaxometry could be used to detect pH changes due to surface electric fields induced by pH changes.[48] However, it was discussed that the observed changes in $T_1$ in the all-optical measurements were due to the charge fluctuation processes between $NV^-/NV^0$ centers, which can be related to the complex exchange of charges within the fNDs and/or their surface.[49,50] In our case, the fND-NGs are mainly located in the cytosol, which provides neutral pH and a more homogeneous pH distribution than the endo/lysosomes, so the pH-induced $T_1$ shortening is not taken into account. As discussed, $T_1$ relaxometry can detect free radicals independently of their involvement in cellular redox reactions[13] and thus offers the possibility of revealing intracellular radical dynamics in real-time.[18] However, the need for quantum sensing protocols implies repetition. In this study, $T_1$ relaxometry measurements are performed continuously and the cumulative optical signals at specified intervals are preserved for the analysis of $T_1$ at a specific time point. This approach is referred to as "pseudo real-time $T_1$ relaxometry."

*Pseudo real-time intracellular radical detection during stimulation with bioactive ligands SST, TPP, and TAT*

SST and TPP have been selected because they can potentially stimulate intracellular radical formation via different pathways, while TAT was set as the negative peptide control since there are no direct connections between TAT and cellular radicals. First, the influence of the $T_1$ of the bioactive ligands was assessed in blank control experiments, in which SST, TPP, or TAT were added following a similar procedure but without cells. **Figure S2** indicated that SST, TPP, and TAT did not induce any significant fluctuations of $T_1$, which confirms that any changes in the $T_1$

fluctuation would not be a result of the ligand but rather of the induced cellular response.

Next, fND-NGs-based relaxometry was used to investigate the impact of these ligands on intracellular radical formation. To achieve pseudo real time detection of intracellular radicals, $T_1$ was first calculated as reference $T_1$ ($T_{1\_ref}$) after integration time of t to get a good signal-to-noise ratio. After further signal accumulation at interval time Δt, we calculated $T_1$ ($T_{1\_t+\Delta t}$), in the period of t + Δt, then $T_{1\_t+\Delta t}$ is normalized to $T_{1\_ref}$ to present the $T_1$ change in the interval time Δt, so that we can record the $T_1$ change continuously. This approach is referred to as "pseudo real-time $T_1$ relaxometry." In this study, SST, TPP, or TAT were added during the $T_1$ relaxometry measurements. Briefly, the initial cellular free radical load was measured by $T_1$ relaxometry measurements by the fND-NGs (with counts from 1 M/s to 3 M/s) for 15 min. Subsequently, low concentrations of SST (final concentration of 0.5 µM), TPP (final concentration: 5 µM), or TAT (final concentration: 0.5 µM) were introduced to the cells during the continuous $T_1$ relaxometry measurements, which were performed for a total period of 60 minutes. This concentration of SST was reported to initiate an effect on intracellular NO generation,[34] and the same concentration was used for the negative control peptide, TAT. The used TPP concentration was chosen as it is the concentration that inhibites cellular oxygen consumption rate (OCR).[37] The $T_1$ of the selected intracellular fND-NGs were analyzed at specific time points post-treatment. To study early occurrence of cellular free radicals, every minute of the first 10 min, every 5 minutes of the first 30 min, and every 10 minutes of the subsequent 30-60 min post-treatment were set for $T_1$ relaxometry measurements. Afterward, the same experiments were conducted at higher concentrations (200 times of the lower concentrations) to evaluate whether there was a concentration-dependent effect on radical formation. Here, 10 µL of SST (final concentration: 100 µM), TPP (final concentration: 1mM), or TAT (final concentration: 100 µM) were added to the cells and the same protocol was used as described above. These concentrations of SST, TPP, and TAT are the highest concentrations determined by the cell toxicity assay, where concentrations of SST, TPP, and TAT show no significant cytotoxicity (**Figure S1**). Each experiment was replicated five times to ensure the reliability and reproducibility of the measured $T_1$. The negative control group consisted of cells treated with 10 µL of Dulbecco's phosphate-buffered saline (DPBS), which was performed 3 times. It is

important to mention that due to the constant concentration of DPBS, only measurements of 15 and another 60 minutes were conducted for each particle in the control group (**Figure S3**).

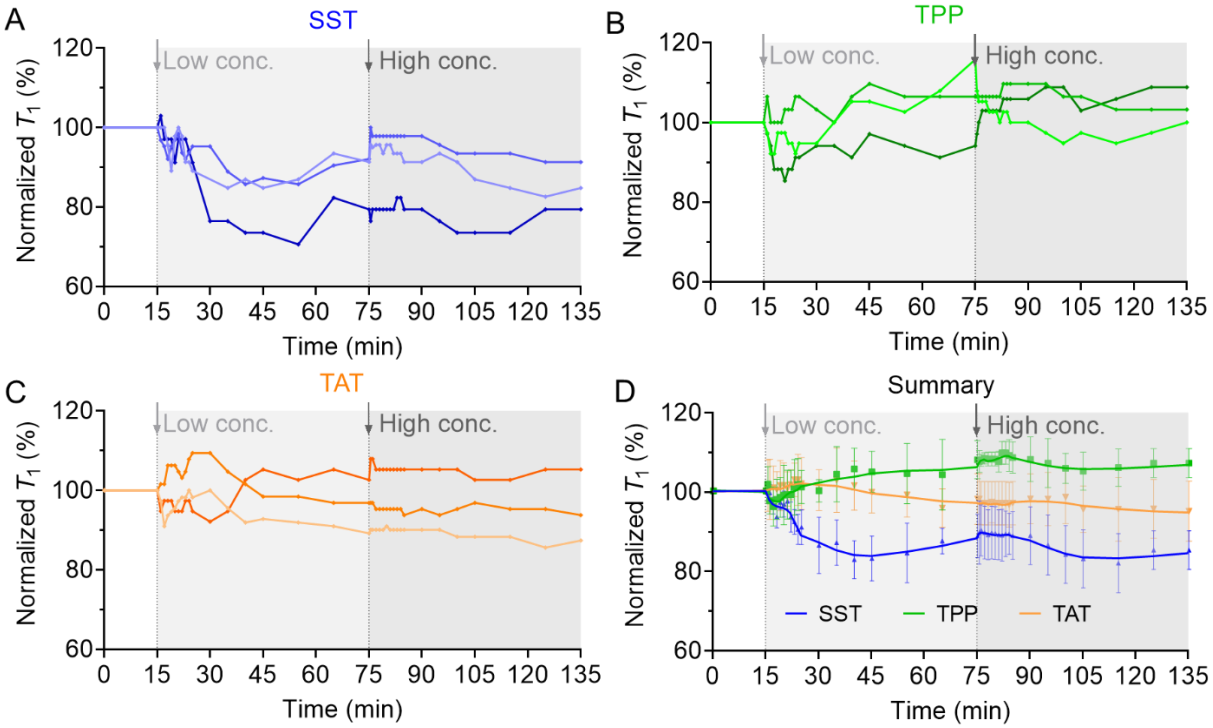


**Figure 3**. Cellular radical response to low and high concentrations of SST (A), TPP (B), and TAT (C) was measured by $T_1$ relaxometry. Three representative curves of each group were presented. (D) The general trend of cellular response to SST, TPP, and TAT treatment. The data is shown as mean ± SD (n=5).

Upon the introduction of low concentrations of SST (0.5 μM), an immediate decline in $T_1$ values was observed in 10 min, and a further reduction of approximately 20% in $T_1$ values was reached within a time frame of approximately 15 – 40 min (**Figure 3a**). It reveals an immediate increase in the amount of intracellular radicals in 10 min and it increases by approximately 20% after 40 minutes. To test whether the amount of intracellular radical would further increase with increasing of SST concentration, we increased the concentration of SST to 100 μM and found that the $T_1$ did not decrease further, which indicates that the amount of cytoplasmic free radicals was saturated[51]. The possible underlying mechanism could be that SSTRs on the surface of A549 were activated which inhibited NOS expression, consequently causing the significant reduction of NO,[34,52-54] which acts as a counter role of $\bullet O_2^-$ to form non-paramagnetic peroxynitrite ($ONOO^-$) inside the cells. Once the reduction of

NO happened, the process will be reversed to maintain the balance of NO and overproducing $\bullet O_2^-$.[5]

In the second experimental approach, TPP treatment (5 μM and 1 mM) induced a slight increase in $T_1$ (**Figure 3b**), which refers to a potential decrease in the amount of intracellular radical. It has been reported that TPP (1 μM) could potentially influence the mitochondrial respiratory chain complex I, resulting in inhibitory effects on the electron transport chain, consequently affecting the OCR.[37] When OCR decreased, the whole organismal ROS (containing paramagnetic $\bullet O_2^-$, •OH, et al.) production would decrease correspondingly.[36,55]

TAT was used as a negative control since no impact on intracellular pathways involved in radical formation has been reported. Interestingly, $T_1$ relaxometry also showed that there was no significant increase in free radical generation during the membrane pass-through process (**Figure 3C**), which has been found to occur within 5 to 20 minutes.[56]

## Conclusion

In this study, we have demonstrated the utility of nanodiamond relaxometry to study unprecedented details of free radical response upon targeting moieties treatment. We have developed a pseudo real-time intracellular radical detection method, which allows us to monitor the intracellular free radical response of cells at an early stage under the treatment of SST, TPP, and TAT. We found that SST can upregulate the level of intracellular free radicals. In contrast, TPP show downregulation of the level of intracellular free radical. The TAT did not show any cellular radical response during the membrane penetration process since it is not involved in processes directly regulating intracellular radicals. This type of real-time, early-stage radical response under treatment with targeting molecules has not been achieved before. We believe that our method opens a new avenue of understanding the influence of targeting molecules on the role of free radicals in cells and will further our understanding of the fundamental role of various biomolecules and drugs in the formation and scavenging of free radicals in biology.

However, as a newly developed quantum technology, the $T_1$ relaxometry used in this study can only identify the overall cellular response and cannot distinguish specific free radical species. Thereby, sophisticated pulsing techniques such as

double electron-electron resonance, can then be developed to identify specific free radical species to enhance specificities. Besides, the theoretical model can be improved to more accurately quantify the number of radicals in living cells, providing more detailed information to understand radical-related signaling pathways. These improvements will bring us into the era of quantum biology.

## Disclosure statement

No potential conflict of interest was reported by the authors.


## Acknowledgement

The authors thank Laura Cheng for her assistance with the $T_1$ relaxometry measurement. T. Weil and F. Jelezko are grateful for the financial support from the Deutsche Forschungsgemeinschaft (DFG, German Research Foundation) - Project number 316249678 - SFB 1279 (C04), and Carl Zeiss Foundation – project Ultrasens-Vir. F. Jelezko acknowledges the financial support from European Research Council (ERC) - Project HyperQ (grant no 856432), German Federal Ministry of Education and Research (BMBF) - Project DiaQNOS and QSens (grant no 03ZU1110FF).

## Reference


1. G. Pizzino, N. Irrera, M. Cucinotta, et al.. Oxidative stress: Harms and benefits for human health. *Oxidative Med. Cell. Longev.* **2017**; 2017: 8416763.
2. V. Lobo, A. Patil, A. Phatak, et al.. Free radicals, antioxidants and functional foods: Impact on human health. *Phcog. Rev.* **2010**; 4(8): 118-126.
3. F. Okada. Inflammation and free radicals in tumor development and progression. *Redox Rep.* **2002**; 7(6): 357-368.
4. C. Nathan and A. Cunningham-Bussel. Beyond oxidative stress: An immunologist's guide to reactive oxygen species. *Nat. Rev. Immunol.* **2013**; 13(5): 349-361.
5. R. Radi. Oxygen radicals, nitric oxide, and peroxynitrite: Redox pathways in molecular medicine. *Proc. Natl. Acad. Sci. U. S. A.* **2018**; 115(23): 5839-5848.
6. J. A. Knight. Review: Free radicals, antioxidants, and the immune system. *Ann. Clin. Lab. Sci.* **2000**; 30(2): 145-158.
7. C. Andres, J. M. Perez De La Lastra, C. Juan, et al.. The role of reactive species on innate immunity. *Vaccines* **2022**; 10(10): 1735.
8. A. Gomes, E. Fernandes, and J. L. Lima. Fluorescence probes used for detection of reactive oxygen species. *J. Biochem. Biophys. Methods* **2005**; 65(2-3): 45-80.
9. V. G. Damle, K. Wu, D. J. Arouri, et al.. Detecting free radicals post viral infections. *Free Radic. Biol. Med.* **2022**; 191: 8-23.
10. B. Kalyanaraman, V. Darley-Usmar, K. J. Davies, et al.. Measuring reactive oxygen and nitrogen species with fluorescent probes: Challenges and limitations. *Free Radic. Biol. Med.* **2012**; 52(1): 1-6.
11. Y. Wu and T. Weil. Recent developments of nanodiamond quantum sensors for biological applications. *Adv. Sci.* **2022**; 9(19): 2200059.
12. R. Schirhagl, K. Chang, M. Loretz, et al.. Nitrogen-vacancy centers in diamond: Nanoscale sensors for physics and biology. *Annu. Rev. Phys. Chem.* **2014**; 65: 83-105.
13. S. Steinert, F. Ziem, L. T. Hall, et al.. Magnetic spin imaging under ambient conditions with sub-cellular resolution. *Nat. Commun.* **2013**; 4: 1607.
14. V. Vaijayanthimala, Y. Tzeng, H. Chang, et al.. The biocompatibility of fluorescent nanodiamonds and their mechanism of cellular uptake. *Nanotechnology* **2009**; 20(42): 425103.
15. J. Barton, M. Gulka, J. Tarabek, et al.. Nanoscale dynamic readout of a chemical redox process using radicals coupled with nitrogen-vacancy centers in nanodiamonds. *ACS Nano* **2020**; 14(10): 12938-12950.
16. Y. Wu, P. Balasubramanian, Z. Wang, et al.. Detection of few hydrogen peroxide molecules using self-reporting fluorescent nanodiamond quantum sensors. *J. Am. Chem. Soc.* **2022**; 144(28): 12642-12651.
17. A. Sigaeva, H. Shirzad, F. P. Martinez, et al.. Diamond-based nanoscale quantum relaxometry for sensing free radical production in cells. *Small* **2022**; 18(44): 2105750.
18. A. Sigaeva, N. Norouzi, and R. Schirhagl. Intracellular relaxometry, challenges, and future directions. *ACS Cent. Sci.* **2022**; 8(11): 1484–1489.
19. L. Nie, A. C. Nusantara, V. G. Damle, et al.. Quantum monitoring of cellular metabolic activities in single mitochondria. *Sci. Adv.* **2021**; 7(21): eabf0573.
20. K. Wu, T. A. Vedelaar, V. G. Damle, et al.. Applying NV center-based quantum sensing to study intracellular free radical response upon viral infections. *Redox Biol.* **2022**; 52: 102279.
21. K. Wu, L. Nie, A. C. Nusantara, et al.. Diamond relaxometry as a tool to investigate the free radical dialogue between macrophages and bacteria. *ACS Nano* **2023**; 17(2): 1100-1111.
22. Q. Lu, B. Vosberg, Z. Wang, et al.. Unraveling eumelanin radical formation by nanodiamond optical relaxometry in a living cell. Preprint **2023**; DOI: 10.26434/chemrxiv-2023-7bb5k.

23. Y. Wu, M. N. A. Alam, P. Balasubramanian, et al.. Nanodiamond theranostic for light-controlled intracellular heating and nanoscale temperature sensing. *Nano Lett.* **2021**; 21(9): 3780-3788.
24. Y. Wu, M. N. A. Alam, P. Balasubramanian, et al.. Fluorescent nanodiamond–nanogels for nanoscale sensing and photodynamic applications. *Adv. Biomed. Res.* **2021**; 1(7): 2000101.
25. M. Theodoropoulou and G. K. Stalla. Somatostatin receptors: From signaling to clinical practice. *Front. Neuroendocrinol.* **2013**; 34(3): 228-252.
26. J. Zielonka, J. Joseph, A. Sikora, et al.. Mitochondria-targeted triphenylphosphonium-based compounds: Syntheses, mechanisms of action, and therapeutic and diagnostic applications. *Chem. Rev.* **2017**; 117(15): 10043-10120.
27. J. M. Gump and S. F. Dowdy. TAT transduction: The molecular mechanism and therapeutic prospects. *Trends Mol. Med*. **2007**; 13(10): 443-448.
28. H. S. Jung, K. J. Cho, Y. Seol, et al.. Polydopamine encapsulation of fluorescent nanodiamonds for biomedical applications. *Adv. Funct. Mater.* **2018**; 28(33): 1801252.
29. B. H. Shamsi, M. Chatoo, X. Xu, et al.. Versatile functions of somatostatin and somatostatin receptors in the gastrointestinal system. *Front. Endocrinol.* **2021**; 12: 652363.
30. C. Bousquet, E. Puente, L. Buscail, et al.. Antiproliferative effect of somatostatin and analogs. *Chemotherapy* **2001**; 47: 30-39.
31. Y. Zou, X. Xiao, Y. Li, et al.. Somatostatin analogues inhibit cancer cell proliferation in an SSTR2-dependent manner via both cytostatic and cytotoxic pathways. *Oncol. Rep.* **2009**; 21(2): 379-386.
32. L. Sun and D. H. Coy. Somatostatin receptor-targeted anti-cancer therapy. *Curr. Drug Deliv.* **2011**; 8(1): 2-10.
33. C. Grotzinger and B. Wiedenmann. Somatostatin receptor targeting for tumor imaging and therapy. *Ann. N. Y. Acad. Sci.* **2004**; 1014(1): 258-264.
34. S. Arena, A. Pattarozzi, A. Corsaro, et al.. Somatostatin receptor subtype-dependent regulation of nitric oxide release: Involvement of different intracellular pathways. *Mol. Endocrinol.* **2005**; 19(1): 255-267.
35. T. Akaike and H. Maeda. Nitric oxide and virus infection. *Immunology* **2000**; 101(3): 300-308.
36. C. Hou, N. B. Metcalfe, and K. Salin. Is mitochondrial reactive oxygen species production proportional to oxygen consumption? A theoretical consideration. *Bioessays* **2021**; 43(4): e2000165.
37. C. Reily, T. Mitchell, B. K. Chacko, et al.. Mitochondrially targeted compounds and their impact on cellular bioenergetics. *Redox Biol.* **2013**; 1(1): 86-93.
38. A. D. Frankel and C. O. Pabo. Cellular uptake of the TAT protein from human immunodeficiency virus. *Cell* **1988**; 55(6): 1189-1193.
39. M. Green and P. M. Loewenstein. Autonomous functional domains of chemically synthesized human immunodeficiency virus TAT trans-activator protein. *Cell* **1988**; 55(6): 1179-1188.
40. Y. Kuroda, N. Kato-Kogoe, E. Tasaki, et al.. Oligopeptides derived from autophosphorylation sites of EGF receptor suppress EGF-stimulated responses in human lung carcinoma a549 cells. *Eur. J. Pharmacol.* **2013**; 698(1-3): 87-94.
41. I. Ruseska and A. Zimmer. Internalization mechanisms of cell-penetrating peptides. *Beilstein J. Nanotechnol.* **2020**; 11: 101-123.
42. P. Sarder and A. Nehorai. Deconvolution methods for 3-D fluorescence microscopy images. *IEEE Signal Process. Mag.* **2006**; 23(3): 32-45.
43. K. W. Dunn, M. M. Kamocka, and J. H. Mcdonald. A practical guide to evaluating colocalization in biological microscopy. *Am. J. Physiol. Cell Physiol.* **2011**; 300(4): C723-C742.
44. Y. Zhang, R. Sharmin, A. Sigaeva, et al.. Not all cells are created equal - endosomal escape in fluorescent nanodiamonds in different cells. *Nanoscale* **2021**; 13(31): 13294-13300.

45. W. Stauffer, H. Sheng, and H. Lim. Ezcolocalization: An imagej plugin for visualizing and measuring colocalization in cells and organisms. *Sci. Rep.* **2018**; 8(1): 15764.
46. T. F. Martens, K. Remaut, J. Demeester, et al.. Intracellular delivery of nanomaterials: How to catch endosomal escape in the act. *Nano Today* **2014**; 9(3): 344-364.
47. J. M. Binder, A. Stark, N. Tomek, et al.. Qudi: A modular python suite for experiment control and data processing. *SoftwareX* **2017**; 6: 85-90.
48. T. Yanagi, K. Kaminaga, M. Suzuki, et al.. All-optical wide-field selective imaging of fluorescent nanodiamonds in cells, in vivo and ex vivo. *ACS Nano* **2021**; 15(8): 12869-12879.
49. D. Bluvstein, Z. Zhang, and A. C. B. Jayich. Identifying and mitigating charge instabilities in shallow diamond nitrogen-vacancy centers. *Phys. Rev. Lett.* **2019**; 122(7): 076101.
50. I. Barbosa, J. Gutsche, and A. Widera. Impact of charge conversion on NV- center relaxometry. *Phys. Rev. B.* **2023**; 108(7): 075411.
51. P. Barnett. Somatostatin and somatostatin receptor physiology. *Endocrine* **2003**; 20(3): 255-264.
52. L. J. Hofland and S. W. Lamberts. The pathophysiological consequences of somatostatin receptor internalization and resistance. *Endocr. Rev.* **2003**; 24(1): 28-47.
53. M. Cakir, D. Dworakowska, and A. Grossman. Somatostatin receptor biology in neuroendocrine and pituitary tumours: Part 1-molecular pathways. *J. Cell. Mol. Med.* **2010**; 14(11): 2570-2584.
54. R. E. White, A. Schonbrunn, and D. L. Armstrong. Somatostatin stimulates Ca2+ -activated K+ channels through protein dephosphorylation. *Nature* **1991**; 351(6327): 570-573.
55. E. J. Choi, C. H. Jeon, and I. K. Lee. Ferric ammonium citrate upregulates PD-L1 expression through generation of reactive oxygen species. *J. Immunol. Res.* **2022**; 2022: 6284124
56. M. Zorko and U. Langel. Cell-penetrating peptides: Mechanism and kinetics of cargo delivery. *Adv. Drug Deliv. Rev.* **2005**; 57(4): 529-545.